

Textural transformations in islands on free standing Smectic C* liquid crystal films

Jong-Bong Lee*, Dmitri Konovalov† and Robert B. Meyer

The Martin fisher school of physics,

Brandeis University, Waltham, MA 02454 USA

(Dated: December 2, 2024)

Abstract

We report on and analyze the textural transformations in islands, thicker circular domains, floating in very thin free standing chiral Smectic C* liquid crystal films. As an island is growing, an initial pure bend texture of the c-director changes into a reversing spiral at a critical size. Another distinct spiral texture is induced by changing the boundary condition at the central point defect in the island. To understand these transformations from a pure bend island, a linear stability analysis of the c-director free energy is developed, which predicts a state diagram for the island. Our observations are consistent with the theoretical phase diagram.

PACS numbers: 61.30.Dk, 61.30.Eb, 61.30.Jf

* Present Address: Harvard Medical School, Department of Biological Chemistry and Molecular Pharmacology, Boston, MA 02115

† Present Address: Photon Dynamics Inc., 5970 Optical Court, San Jose, CA 95138

I. INTRODUCTION

Defects and singularities of the director field in two dimensional (2D) ordered molecular systems with in-plane orientational order cause fascinating textures, easily visible by means of polarized-light microscopy. In this paper we report a detailed experimental and theoretical study of a set of simple textural transformations in a system formed by blowing smoke over a thin free standing film of chiral smectic C (SmC^*) liquid crystal. Sub-micron smoke particles nucleate islands, circular regions of added smectic layers, which grow to a certain equilibrium size, with the smoke particle as a point disclination at the center of the island. The island maintains azimuthal symmetry during growth, initially with the c-director field, a unit vector \hat{c} , defined by the projection of the tilted long molecular axis onto the layer, tangentially oriented. We find that this initially stable pure bend texture can transform to two other equilibrium spiral splay-bend textures, either as the islands grow, or when they are momentarily perturbed by external forces. To understand these transformations among stable or metastable textures, we develop a linear stability analysis for this general class of textures, which predicts a state diagram, as a function of island radius, that agrees well with our observations.

Important precursors to this work include an initial report of these phenomena[1], the report of a reversing spiral texture first discovered in domains at the air/water interface when the SmC^* film is both polar and chiral[2], and study of the boojum, a point disclination occurring at the edge of a circular domain[3, 4]. The theoretical analysis of the stability of textures around topological defects has been investigated for Langmuir monolayers with a tilted phase and for free standing Sm C films[5, 6, 7, 8]. Especially important, K. K. Loh *et al.*[9] pointed out that there can be more than one stable or metastable texture for a point defect centered in a circular domain, and described the reversing spiral texture of a circular domain in a chiral system, which can be energetically stable or metastable. The remarkable growth of islands to an equilibrium size, once they are nucleated, is a consequence of their chirality and their resulting polar (ferroelectric) symmetry.[1]

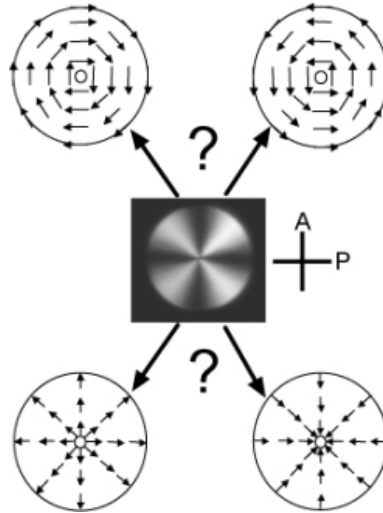


FIG. 1: Tangential or radial? An island observed with crossed polarizers and four possible \hat{c} director configurations, tangential (clockwise or counterclockwise) or radial (outward or inward).

II. TEXTURAL TRANSFORMATIONS OF ISLANDS

Samples are prepared by drawing a small amount of smectic C* liquid crystal material across a 6 mm diameter hole in a thin metal sheet. Materials were prepared from the CS series of mixtures available from Chisso Co. Typical films as drawn were on the order of 10 smectic layers thick.[10] To create islands, smoke from burning paper was wafted across the film. Watching the sample using a polarizing microscope with crossed polarizers, one could observe the growth of islands nucleated by some of the smoke particles. The islands were brighter than the very dark background film, their brightness being proportional to their thickness. Once nucleated, islands grew in area but not in thickness. As the islands grew, one could observe their internal texture due to their birefringence. Although sometimes the smoke particle was the center of a point defect at the periphery of the island, a so-called boojum, most often the sub-visible smoke particle was centered in the island as a +1 point disclination, as shown in Fig. 1.

There are four possible textures for the intensity pattern shown in Fig. 1. For a SmC* film of thickness d with angle ψ between \hat{c} and either of the polarizers, with crossed polarizers, the intensity of transmitted light is

$$I = I_0 \sin^2 2\psi \sin^2 \left(\frac{\pi \Delta n d}{\lambda} \right), \quad (1)$$

where λ is a wavelength of the incident light and Δn is a birefringence for light propagating

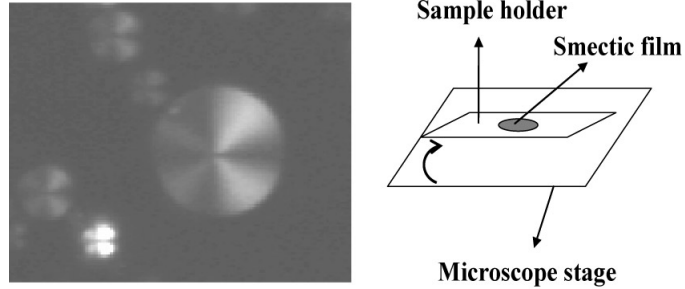


FIG. 2: Islands observed when the lower edge of the sample holder is raised with respect to the microscope stage by about 10° . The texture is tangential counterclockwise.

normal to the film.

We neglect the effects of the twist of \hat{c} through the film thickness, since the islands are thin compared to the helical pitch of the spontaneous twist produced by molecular chirality. The helical pitch in the materials studied was in the range of 3 to 15 micrometers, while the islands were in the range of thickness of 0.06 to 0.15 micrometers.[10] If the \hat{c} director is parallel to either of the polarizers, $\psi = 0, \pi$ or $\pm\pi/2$, then $I = 0$. At $\psi = \pm\pi/4, \pm3\pi/4$, I is a maximum in Eq. (1). Hence, the four orientations of \hat{c} indicated in Fig. 1 are possible.

To distinguish among these cases, the lower edge of the sample holder is lifted producing a small tilt with respect to the microscope stage. After the floating islands move to the edge of the film due to gravity, their appearance changes to that shown in Fig. 2. The increased intensity on the right half of the islands indicates that their c-director texture is tangential counterclockwise, since in that case, the added tilt increases the molecular tilt, relative to the propagation direction of the light, and thus the apparent birefringence, on the right, and decreases it on the left of the center. All the +1 central defect islands, as shown in Fig. 1, have this “pure bend” texture throughout the island.

To explore the stability of pure bend islands, which are apparently at equilibrium, we blew on the film with a small jet of gas. The resulting swirling often induced two kinds of distinct changes from a pure bend texture. In all cases the boundary condition at the outer edge of the island remained tangential counterclockwise. However, the boundary condition at the smoke particle at the core of the point defect would (a) sometimes change from tangential to approximately radial, or (b) remain tangential. Right after blowing, there was often a very tightly wound spiral in the texture, which slowly relaxed to equilibrium, as shown in Fig. 3. Over the course of minutes, as the c-director relaxes, in case (a) this texture

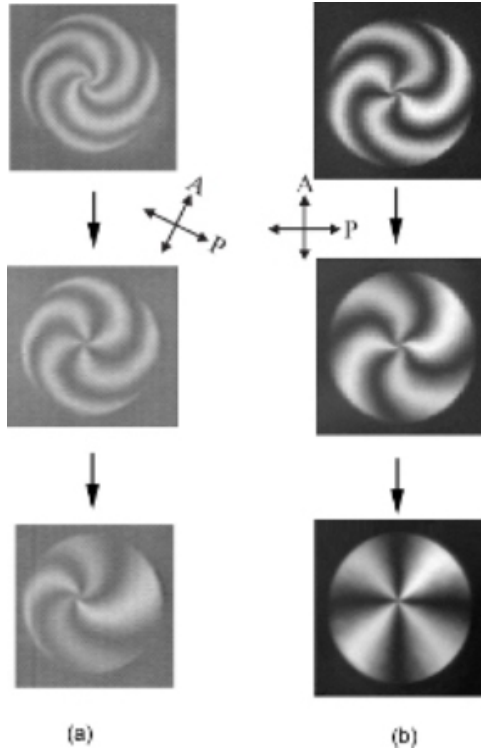


FIG. 3: The textures after blowing on islands with pure bend texture. (a) A pure bend island switches to a 'simple spiral' with radial c-director at the core. (b) A pure bend island exhibits a transient (unstable) reversing spiral texture, when the core boundary condition is unchanged.

equilibrates to a final state with roughly $\pm\pi/2$ rotation from radial at the core to tangential at the outer boundary (Bottom of Fig. 3(a)). We call this spiral texture a "simple spiral". We have observed the simple spirals with radial inward or outward boundary conditions at the core, and right or left handed spirals. Neither the sense of the spiral nor the sign of the radial boundary condition is meaningful, since observing the sample from the other side would clearly reverse both these characteristics. There is a size-dependence in this textural transformation; pure bend islands of a small size are hardly ever transformed into simple spirals. This indicates that there is only a small interaction energy between the molecular orientation and the smoke particle, since the pure bend texture is being stabilized by the torque transmitted from the outer island boundary to the defect core.

However the other spiral texture resulting from blowing, case (b), which maintains its tangential boundary condition at the core, which we call a 'reversing spiral', goes back to the pure bend texture, as shown in Fig. 3(b), when it started from an apparently stable pure bend texture.

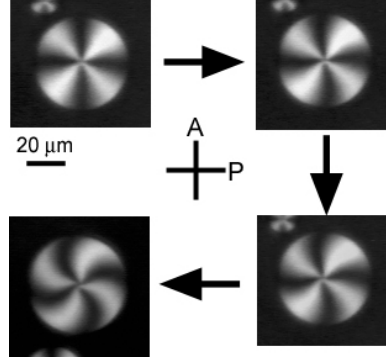


FIG. 4: Transformation of a pure bend island into a reversing spiral island. It took around 30 min.

Remarkably, as shown in Fig. 4, as a stable pure bend island grows, at some critical size the c-director texture spontaneously starts to evolve into a reversing spiral. This transition is driven by a competition between the bend and splay elastic energies. If the splay elastic constant is less than the bend constant, this enables the transformation from a pure bend texture to a reversing spiral in a large enough island. The time it takes to reach equilibrium depends on the thickness of the island. The thinner the island, the less time. It took 30 minutes for the pure bend island in Fig. 4 to reach equilibrium.

III. LINEAR STABILITY ANALYSIS

To explore the stability of the texture in the islands, we employ linear stability analysis. To find the equilibrium configuration of \hat{c} in the islands, we should minimize the following free energy consisting of an integral of the elastic energy density over the area of the island, and the edge energy at the sample boundaries.

$$F = \int [K_s(\nabla \cdot \hat{c})^2 + K_b(\nabla \times \hat{c})^2]dA + \oint \sigma(\phi)dl. \quad (2)$$

ϕ is defined as the angle between \hat{c} and the outward radial vector \hat{r} . $\sigma(\phi)$ is the anisotropic energy per unit length of edge. Note that it is a periodic function, $\sigma(\phi - 2\pi) = \sigma(\phi)$. Generally it is written as

$$\sigma(\phi) = \sigma_0 + \sum_{n=1}^{\infty} [a_n \cos(n\phi) + c_n \sin(n\phi)], \quad (3)$$

in which σ_0 is an isotropic term [5, 11]. In the areal free energy density, the possible linear terms, $\nabla \cdot \hat{c}$ and $\nabla \times \hat{c}$, are converted to line energies by the divergence theorem

and Stoke's theorem. Therefore the first order terms $a_1 \cos \phi$ and $c_1 \sin \phi$ in Eq. (3) arise from a spontaneous splay($\nabla \cdot \hat{c}$) and a spontaneous bend($\nabla \times \hat{c}$) respectively. However in a free-standing film, which is physically the same when viewed from the top or bottom, no spontaneous splay of \hat{c} is possible; for films floating on a liquid this term is allowed [2] by the polar symmetry of the sample. So a_1 must vanish. c_1 arises directly from the spontaneous bending (in our case, left turning) produced by the molecular chirality in the SmC*, and it is directly responsible for the minimum energy textures having a counterclockwise tangential boundary condition at the outer edge of all the islands we observed. We include in $\sigma(\phi)$ only the lowest terms for the line energy,

$$\sigma(\phi) = \sigma_0 + a_2 \cos 2\phi + c_1 \sin \phi. \quad (4)$$

For the islands we have created by a heterogeneous nucleation with a strong anchoring tangential boundary condition at $r = R$ (outer radius of island) and a weak anchoring boundary at $r = \epsilon$ (radius of the particle at the center), the line energy is

$$\oint \sigma(\phi) dl = 2\pi R \sigma\left(\frac{\pi}{2}\right) + 2\pi \epsilon \sigma(\phi(\epsilon)). \quad (5)$$

The first term on the right side is the line energy for the outer boundary and the second is for the inner boundary. The total free energy for a island in Eq. (2) can be rewritten as the sum of the areal elastic free energy and the line energy of Eq. (5) in terms of $x \equiv \ln(r/\epsilon)$.

$$\begin{aligned} F = \pi K \int_0^{x_0} & \left[\left(1 + \mu \cos 2\phi\right) \left(\frac{d\phi}{dx}\right)^2 + 2\mu \sin 2\phi \frac{d\phi}{dx} \right. \\ & \left. + (1 - \mu \cos 2\phi) \right] dx + 2\pi \epsilon \sigma(\phi(0)), \end{aligned} \quad (6)$$

where,

$$\begin{aligned} x_0 & \equiv \ln(R/\epsilon), \\ K & \equiv \frac{K_s + K_b}{2}, \\ \mu & \equiv \frac{-K_s + K_b}{K_s + K_b}. \end{aligned}$$

The constant term $2\pi R \sigma(\pi/2)$ in the total free energy is ignored, because it has no effect on $\phi(x)$. Here we assume that the radial configuration of the \hat{c} director, $\phi = 0$ or $\phi = \pi$, in the areal free energy is a state for minimum energy, based on our observation that \hat{c} tends to rotate toward a radial orientation in large enough islands. Hence $K_s < K_b$, which means μ ranges from 0 to less than 1.

The equilibrium condition for $\phi(x)$ from the Euler-Lagrange equation derived from Eq. (6) is

$$(1 + \mu \cos 2\phi) \frac{d^2\phi}{dx^2} - \mu \sin 2\phi \left(\frac{d\phi}{dx} \right)^2 - \mu \sin 2\phi = 0. \quad (7)$$

The boundary condition at $x = 0$ obtained from $\left(\frac{\partial \eta(\phi)}{\partial \phi} - \frac{\partial f}{\partial \phi'} \right) \Big|_{x=0} = 0$ is

$$K \left[(1 + \mu \cos 2\phi) \left(\frac{d\phi}{dx} \right) + \mu \sin 2\phi \right] \Big|_{x=0} = \epsilon \frac{d\sigma}{d\phi} \Big|_{x=0}, \quad (8)$$

where f and η are the areal and edge free energy densities.

We found $\phi(x)$ numerically, using strong anchoring at the outer boundary, $\phi(x_0) = \pi/2$, as required by our observation. However, depending on the choice of parameters, there might be one or more numerical solutions. Linear stability analysis is used to determine if these solutions define local minima for the free energy. For the analysis, we need to manipulate the total energy in Eq. (6). Defining

$$A(\phi) \equiv 1 + \mu \cos 2\phi, \quad (9)$$

$$B(\phi) \equiv 2\mu \sin 2\phi, \quad (10)$$

$$C(\phi) \equiv 1 - \mu \cos 2\phi, \quad (11)$$

Eq. (6) can be rewritten as

$$F = \pi K \int_0^{x_0} dx \left[A(\phi) \left(\frac{d\phi}{dx} \right)^2 + B(\phi) \frac{d\phi}{dx} + C(\phi) \right] + 2\pi\epsilon\sigma(\phi(0)). \quad (12)$$

Let's start with the second term in the integral.

$$\begin{aligned} \pi K \int_0^{x_0} B(\phi) \frac{d\phi}{dx} dx &= \pi K \int_{\phi(0)}^{\phi(x_0)} B(\phi) d\phi \\ &= \pi K \mu (\cos 2\phi(0) - \cos 2\phi(x_0)) \\ &= \pi K \mu (\cos 2\phi(0) + 1). \end{aligned} \quad (13)$$

We rewrite Eq. (12).

$$F = \pi K \int_0^{x_0} \left[A(\phi) \left(\frac{d\phi}{dx} \right)^2 + C(\phi) \right] dx + \frac{1}{2} \pi K S(\phi(0)), \quad (14)$$

where $\frac{1}{2} \pi K S(\phi(0)) \equiv 2\pi\epsilon\sigma(\phi(0)) + \pi K \mu \cos(2\phi(0)) + \pi K \mu$. We next incorporate the line energy into the integral and symmetrize the problem around $x = 0$, obtaining

$$F = \frac{1}{2} \int_{-x_0}^{x_0} \left[A(\phi) \left(\frac{d\phi}{dx} \right)^2 + C(\phi) + \delta(x) S(\phi(x)) \right] dx, \quad (15)$$

in which $\delta(x)$ is a Dirac delta function.

Now we expand the above free energy to second order in a small fluctuation $\varphi = \phi - \phi_0$, in which ϕ_0 is a solution that makes the total free energy F an extremum. The boundary conditions are $\varphi(-x_0) = \varphi(x_0) = 0$ due to the strong anchoring. The expanded free energy δF is

$$\begin{aligned} \delta F = & \frac{1}{2}\pi K \int_{-x_0}^{x_0} \left\{ \left[A(\phi_0) + A'(\phi_0)\varphi + \frac{1}{2}A''(\phi_0)\varphi^2 \right] \left[\left(\frac{d\phi_0}{dx} \right)^2 + 2\frac{d\phi_0}{dx}\frac{d\varphi}{dx} + \left(\frac{d\varphi}{dx} \right)^2 \right] \right. \\ & \left. + \left[C(\phi_0) + C'(\phi_0)\varphi + \frac{1}{2}C''(\phi_0)\varphi^2 \right] + \delta(x) \left(S(\phi_0) + S'(\phi_0)\varphi + \frac{1}{2}S''(\phi_0)\varphi^2 \right) \right\} dx, \end{aligned} \quad (16)$$

where the notation ' and " denote first and second derivatives with respect to ϕ .

Since we are expanding around an extremum solution, the first functional derivative $\delta F_1 = 0$. As a result, the lowest term is the second order derivative of the free energy,

$$\begin{aligned} \delta F_2 = & \frac{1}{2}\pi K \int_{-x_0}^{x_0} \left[\frac{1}{2}A''(\phi_0) \left(\frac{d\phi_0}{dx} \right)^2 \varphi^2 + A(\phi_0) \left(\frac{d\varphi}{dx} \right)^2 \right. \\ & \left. + 2A'(\phi_0) \frac{d\phi_0}{dx} \varphi \frac{d\varphi}{dx} + \frac{1}{2}C''(\phi_0)\varphi^2 + \delta(x) \frac{1}{2}S''(\phi_0)\varphi^2 \right] dx. \end{aligned} \quad (17)$$

We next convert the second derivative terms to a symmetric form by integration by parts.

$$\begin{aligned} A(\phi_0) \left(\frac{d\varphi}{dx} \right)^2 & \rightarrow -A'(\phi_0) \frac{d\phi_0}{dx} \frac{d\varphi}{dx} \varphi - A(\phi_0) \frac{d^2\varphi}{dx^2} \varphi, \\ 2A'(\phi_0) \frac{d\phi_0}{dx} \varphi \frac{d\varphi}{dx} & \rightarrow -A''(\phi_0) \left(\frac{d\phi_0}{dx} \right)^2 \varphi^2 - A'(\phi_0) \frac{d^2\phi_0}{dx^2} \varphi^2. \end{aligned} \quad (18)$$

After substituting Eq. (18) into Eq. (17), we obtain

$$\begin{aligned} \delta F_2 = & \frac{1}{2}\pi K \int_{-x_0}^{x_0} \varphi \left[-\frac{d}{dx} \left(A(\phi_0) \frac{d}{dx} \right) - \frac{1}{2}A''(\phi_0) \left(\frac{d\phi_0}{dx} \right)^2 \right. \\ & \left. - A'(\phi_0) \frac{d^2\phi_0}{dx^2} + \frac{1}{2}C''(\phi_0) + \frac{1}{2}\delta(x)S''(\phi_0(0)) \right] \varphi dx. \end{aligned} \quad (19)$$

δF_2 has the form of

$$\delta F_2 = \frac{1}{2}\pi K \int_{-x_0}^{x_0} [\varphi L\varphi] dx, \quad (20)$$

where L is the operator $-\frac{d}{dx}(A(\phi_0)\frac{d}{dx}) + V(x)$ and $V(x)$ is completely determined by the solution $\phi_0(x)$. This symmetrized second derivative term in L is now Hermitian or self adjoint, as is $V(x)$. The operator L has an infinite set of eigenfunctions which form a complete

orthogonal set of functions for constructing all suitable functions satisfying the boundary conditions on the integral.[12] The eigenfunction with the lowest eigenvalue does not cross zero between the $\pm x_0$ end points, while sequentially, each higher eigenvalue corresponds to an eigenfunction with one more zero crossing. Let's expand a test function φ in the eigenfunctions of L , $\varphi = \sum a_i \varphi_i$, in which φ_i is normalized so that

$$\int_{-x_0}^{x_0} \varphi_i^2 dx = 1, \quad (21)$$

and each eigenfunction φ_i has an eigenvalue C_i . Then

$$\delta F_2 = \int_{-x_0}^{x_0} \varphi L \varphi dx = \sum a_i^2 C_i \quad (22)$$

If the lowest eigenvalue $C_1 > 0$, δF_2 is positive, and ϕ_0 minimizes the free energy with respect to small variations. If $C_1 < 0$, then φ_1 clearly lowers the free energy and ϕ_0 is not a minimizing function. To test a solution ϕ_0 we find the eigenfunction of the operator L , which does not cross zero between the endpoints, and determine its eigenvalue. A negative eigenvalue indicates instability.

IV. RESULTS

We have described the procedures to obtain the equilibrium textures and to examine their stability against infinitesimal fluctuations to understand what we observe, which is that there can be more than one stable or metastable solution, for the texture of an island. To find minima of the free energy, we numerically solve the Euler-Lagrange equation Eq. (7) with the boundary conditions, Eq. (8) at the core and strong anchoring $\phi = \pi/2$ at the outer boundary. We adopt the shooting method, in which starting from the outer boundary with $\phi = \pi/2$, we vary the slope of ϕ , and integrate to the inner boundary. The discrepancy from the desired inner boundary condition is used to adjust the initial slope, repeating until the solution is obtained.

In Fig. 5, we show the free energy of functions ϕ as the slope at the outer boundary is varied. The local minima represent solutions of the Euler-Lagrange equation that satisfy the boundary condition at the inner boundary. For the four island sizes shown, compare the free energy of the pure bend island, with initial slope zero, to that of the other local minima. The global minimum at large initial slope represents a simple spiral, while the

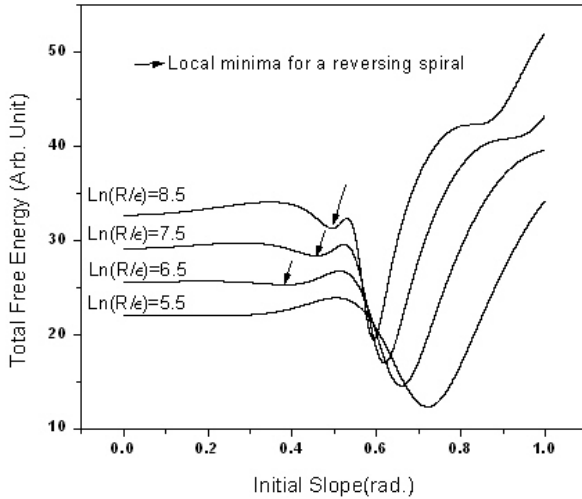


FIG. 5: A plot showing the minima of the free energy of an island as a function of the initial slope of ϕ at the outer boundary for the following parameters, $K = 1$, $\mu = 0.13$, $\epsilon c_1 = 1.0$, and $\epsilon a_2 = 0.6$. At initial slope 0, the free energy is for a pure bend island.

local minimum that appears for island size just above $\ln(R/\epsilon) = 5.5$ is a reversing spiral. Actually many local minima can exist at larger initial slope, but they have much higher free energy than the free energy of the pure bend island. The linear stability analysis of the pure bend texture shows that once the reversing spiral solution appears, the pure bend texture is unstable.

An example of a stable simple spiral is illustrated in Fig. 6. In Fig. 6(a), ϕ varies monotonically from the core to the outer boundary. This is an illustration of the lowest energy configuration for $\mu=0.13$, $K=1$, $\epsilon c_1=1.0$, and $\epsilon a_2=0.6$ at $\log(R/\epsilon)=6.0$. Fig. 6(b) represents the appearance of the island, as seen between crossed polarizers, for which $\phi(x)$ is shown in Fig. 6(a). The island in Fig. 6(c) is a typical simple spiral we created by blowing. Note that in the case calculated here, the stable boundary condition at the core is not radial but almost reversed tangential, but the part of the solution with values of $\phi < 0$ is so close to the core that it is essentially invisible at optical resolution, since the radius of the island is only on the order of 20 micrometers. The important qualitative observation is that ϕ increases monotonically from the core. In fact we do not know the precise core size, just

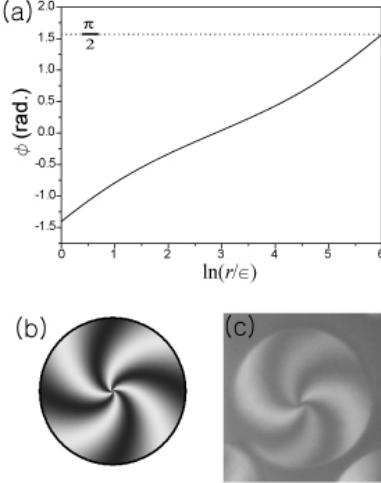


FIG. 6: Stable solution for a simple spiral. $K=1$, $\mu=0.13$, $\epsilon c_1=1.0$, and $\epsilon a_2=0.6$ at $\log(R/\epsilon)=6.0$.

(b) Texture of the solution as seen between crossed polarizers. (c) A simple spiral we observed, after blowing on the sample.

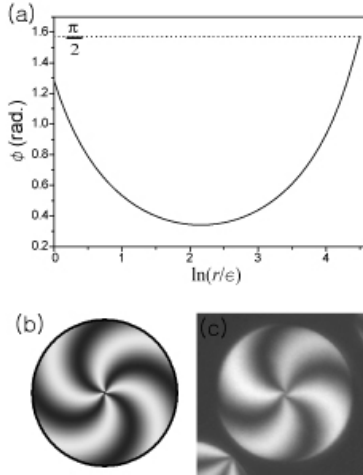


FIG. 7: Stable solution for a reversing spiral. $K=1$, $\mu=0.6$, $\epsilon c_1=1.0$, and $\epsilon a_2=0.5$ at $\log(R/\epsilon)=4.5$.

(b) The texture seen between crossed polarizers. (c) A typical reversing spiral island.

that it is sub-visible.

In the reversing spiral seen in Fig. 7, ϕ rotates in one direction from the inner boundary until reaching a minimum angle, and then rotates in the other direction to match the outer boundary condition. This configuration does not represent an absolute minimum of the free energy, but is locally stable for $\mu=0.6$, $K=1$, $\log(R/\epsilon)=4.5$, $\epsilon c_1=1.0$, and $\epsilon a_2=0.5$. Fig. 7(b) shows the appearance of the island as seen between crossed polarizers, for the solution $\phi(x)$

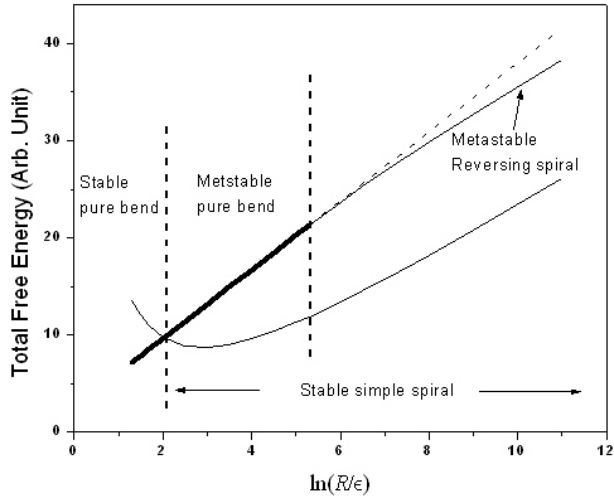


FIG. 8: State diagram for an island. $K=1$, $\mu=0.13$, $\epsilon c_1=1.0$, and $\epsilon a_2=0.6$.

shown in Fig. 7(a). Fig. 7(c) is the texture of an observed reversing spiral. Again, the detailed texture near the core is unresolved, but qualitatively it is clear that the spiral reverses curvature at very small radius.

Fig. 8 is a state diagram for an island, as a function of its radius, obtained by numerical calculation, where the simulation parameters are $K=1$, $\mu=0.13$, $\epsilon c_1=1.0$, and $\epsilon a_2=0.6$. At small radius, the energy for a simple spiral is much higher than the energy of a pure bend texture. This explains why we can't observe the simple spirals in islands of small size. Above a certain size, the pure bend island is only metastable, but there is a sizable energy barrier for transition to the simple spiral. However, above a second critical size, the pure bend island becomes unstable relative to a reversing spiral with a lower energy, without any energy barrier. The transition size is sensitive to K_s and K_b . If K_s and K_b are the same, the size of the transition diverges. The bigger μ , the smaller the size for this second order transition.

For island radius larger than the radius for the crossing of the free energies of the pure bend texture and the simple spiral, around $\ln(R/\epsilon) = 2$ in this case, the pure bend texture can be transformed into a simple spiral as a first order transition. We think blowing on the sample makes this possible in our experiments, because the highly curled transient spiral

state it produces provides the torque needed to change the inner boundary condition. The spiral then relaxes into the stable simple spiral state.

V. DISCUSSION

We have observed the textures of circular islands of a ferroelectric smectic C* liquid crystal, especially studying first and second order transformations of textures as a function of island size. First our basic observations confirm the fact that the chirality of the smectic C* phase induces a preferred bend curvature in the plane of the smectic layers, leading in the case of the materials we studies, to a general left turning bend texture as their ground state. Second, using an elastic model in which the difference of elastic constants, $K_b - K_s$, provides a driving force, and the anchoring of the c-director at the core of the central disclination is weak, we construct a plausible state diagram that agrees with our observations. The circular geometry of the island, combined with the strong tangential anchoring of the c-director at its outer boundary, demand a curved texture, which makes the difference between the splay and bend curvature elastic constants crucial. The continuous transition from the pure bend island to the reversing spiral is completely analogous mathematically to the behavior of a plane parallel sheet of nematic with tangential boundary conditions, in a perpendicular magnetic field. As the sheet grows thicker, at a critical thickness, a continuous Frederiks transition occurs, in which the director rotates toward the external field direction. Here, that effective field direction is radial, converting bend into splay, and lowering the energy.

In studying different materials, using the textural transformation from pure bend to reversing spiral as a diagnostic, we saw a strong correlation between the spontaneous electrical polarization of the ferroelectric phase and the apparent difference between the bend and splay elastic constants; high polarization materials matched our model of a material with a high bend elastic constant. This result correlates well with the fact that bend curvature of the c-director produces divergence of the spontaneous polarization, resulting in space charges which interact to increase the free energy of the bent state. In low frequency, or quasi-static, conditions, the resulting space charge is partially screened by free charges in the material, reducing the otherwise long range electrostatic interactions to an effective local contribution to the free energy, which can be expressed as an increase in the effective bend elastic constant.[13] The fact that our state diagram and the textures we calculate from the

elastic model agree well with our observations leads us to hypothesize that we can approximate the electrostatic interactions and energy by this change of effective elastic constants. To explore this hypothesis further, we made independent studies of the elastic constants and the interactions of bend distortions with free charges in free standing SmC* films, comparing high frequency and quasi-static behavior. To accomplish this, we performed light scattering experiments on c-director fluctuation dynamics, with electric field quenching of fluctuations, with analysis including both bend-induced polarization charge and conduction charge screening. They will be reported elsewhere.

- [1] R.B.Meyer, D.Konovalov, I.Kraus and J.B.Lee, Mol. Cryst. Liq. Cryst. **364** 123-131 (2001).
- [2] I. Kraus and R. B. Meyer, Phys. Rev. Lett. **82**, 3815 (1999).
- [3] C. C. Muzny and N. A. Clark, Phys. Rev. Lett. **68**, 804 (1992).
- [4] J. E. MacLennan, U. Sohling, N. A. Clark, and M. Seul, Phys. Rev. E **49**, 3207 (1994).
- [5] D. Pettey and T. C. Lubensky, Phys. Rev. E **59**, 1834 (1999).
- [6] S. Riviere and J. Meunier, Phys. Rev. Lett. **74**, 2495 (1995).
- [7] J. Fang, E. Teer, C. M. Knobler, K. K. Loh, and J. Rudnick, Phys. Rev. E **56**, (1997).
- [8] S. A. Langer and J. P. Sethna, Phys. Rev. A **34**, 5035 (1986).
- [9] K.-K. Loh, I. Kraus, and R. B. Meyer, Phys. Rev. E **62**, 5115 (2000).
- [10] J.-B. Lee, R. B. Meyer, and R. A. Pelcovits, to be published. J.-B. Lee, Ph.D. thesis, Brandeis University, (2004).
- [11] J. Rudnick and R. Bruinsma, Phys. Rev. Lett. **74**, 2491 (1995).
- [12] For a clear discussion of Sturm Liouville theory see Morse and Feshbach, *Methods of Theoretical Physics*, McGraw-Hill, 1953.
- [13] K. Okano, Jpn. J. Appl. Phys. **25**, L846 (1986).